Land Surface Temperature Estimation of Mandya district using LANDSAT-8 data

Aryalekshmi B N[1,*], Mohammed Ahamed J[2], Dr. R C Biradar[1], and Dr. Chandrasekar K[3]

[1] School of ECE, REVA University, Bangalore, India
[2] RRSC – South, NRSC, ISRO, Bengaluru, India
[3] RRSC-Hyderabad, NRSC, ISRO, India
[*] Corresponding author. E-mail: aryalks88@gmail.com

Received: Dec. 10, 2019, Accepted: May. 29, 2020

This paper focuses on the estimation of LST over Mandya district (120°31'N, 760°53'E), which is a part of the Cauvery river basin in Karnataka, India, using LANDSAT-8 satellite data for 12 meteorological stations. Landsat 8 data is used for experimentation during 21st Jan 2018 and 6th Feb 2018 for LST analysis of identified area. More than half of the land area in the Mandya district is under agricultural use. Fluctuations in LST affects the quality of agricultural production. As a result, proper estimation of LST is very much required for the management of crop growth, development, and yield component. Spectral radiance from band 10 and emissivity of thermal infrared bands was used as input for LST estimation. Surface emissivity was obtained with the help of NDVI (Normalized Difference Vegetation Index), Leaf Area Index (LAI), and Albedo in the Mandya region. ERDAS IMAGINE and ArcGIS software were used for modeling. The obtained data compared with weather station data collected by KSNDMC (Karnataka State Natural Disaster Monitoring Centre). For this analysis, we considered two sets of data taken on different dates during the said period. The Root Mean Square Error (RMSE) and correlation coefficient are used as statistical criteria for evaluating the model efficiency. From the comparison, it is found that RMSE and R for the first date are 0.94°C, 0.62, and for the second date, it is 1.26°C, 0.88, respectively. It is observed that LST and weather data do follow the same pattern for the selected 12 meteorological stations.

Keywords: Emissivity; Land surface temperature (LST); NDVI; LAI; LANDSAT-8; Mandya

http://dx.doi.org/10.6180/jase.202012_23(4).0002

1. Introduction

Land Surface Temperature (LST) is a crucial factor for analyzing many aspects of biology and climate, affecting organisms and ecosystems from local to global scales. It measures the radiative temperature of the surface of the earth. It has many applications in the field of monitoring vegetation, crop yield, evapotranspiration (ET) [1], urban climate change [2–4], forest fire detection [5, 6], etc. [7, 8]. It also helps in estimating soil moisture [9, 10] in the area of interest. For the study of climate variation over many years, surface temperature analysis plays an important role. When the atmosphere is warmer, the chances of evaporation of water from the river, ocean, and land will be more [11]. When the built-up areas that are the concrete zones of any region increases, it completely changes the Land Use Land Cover (LULC) of those cities, making it warmer than their surrounding areas. Urban Heat Island (UHI) is one of the phenomena that occurs due to an increase in temperature. UHI leads to the replacement of the natural vegetation of that region. With the help of satellite-derived data, we can analyze the effect of urbanization as well as UHI. LST estimation helps in analyzing the UHI effect properly [4].

Modeling of the temporal and spatial patterns of LST is required for understanding the environmental impacts of LST. When the dense network of the meteorological station is unavailable in a particular area, the values obtained from satellite imagery can be used as a parameter for analyzing water resource management, agro-environmental studies, etc. Remote sensing-based estimation of surface temperature produces accurate data when compared with the weather station, which is point data [12, 13]. Surface temperature changes rapidly with the change in the geography of the area, such as due to change in vegetation cover, soil type, surface roughness, etc. Due to all these factors, the estimation of LST is an important parameter for the analysis of environmental changes in the whole part of the world.

Many algorithms are proposed for the estimation of LST using different RS data [14–17]. As already discussed, many satellite sources are available for getting environmental information. Among this, LANDSAT-8, which is a part of the Landsat program, is most commonly used for LST estimation due to the free availability of satellite images that helps in, accurate estimation of LST [16, 18]. Landsat-8 level 2 data obtained from the United States Geological Survey (USGS) earth explorer website was used in this study. Since these images were already atmospherically corrected using ground data by USGS, no separate atmospheric correction was done. LANDSAT-8 has got two sensors, the Operational Land Imager (OLI) and Thermal Infrared Sensor (TIRS) [19]. Visible and Near-infrared bands data were provided by band 2-7 of LANDSAT-8; it is of 30m*30m pixel size. Longwave (thermal) radiation data is provided by band-10 and band-11, which are acquired at 100m resolution but are resampled at 30m in delivered data product. From LANDSAT-8, only band-10 is currently used in this study due to uncertainty in calibration reported for band-11 by the USGS [20].

The reason for choosing Mandya district is that agricultural sector is the principal patron of the Indian economy, and Mandya is one of the significant agriculturally flourishing district of Karnataka . The study of LST with satellite data over this region is limited when compared with the other part of the world. The Mandya district lies in the Cauvery river basin, and it shares its border with the districts of Hassan, Mysore, Tumkur, Ramanagara, and Chamarajanagar. The major portion of the total land area of Mandya is under agricultural use. Some of the major crops of this region are ragi, rice, sugarcane, groundnut, sesame, and pulses. One of the major commercial crops of Mandya is Sugarcane. Weather parameters such as temperature, rainfall, evapotranspiration (ET), etc. are important factors for agricultural production. Variation in weather parameters results in a change in the quality of agricultural products. Mainly LST variation will lead to changes in climatic conditions, UHI, less crop yield, etc. As a result, a proper study of the LST of Mandya is required for the agricultural production growth of Karnataka. Estimation of LST from Landsat-8 image for Mandya district is not known as of the time of writing this paper.

The accurate result of LST is mainly based on the type of data, condition of the environment, and the type of algorithm used. The retrieval of LST from remotely sensed TIR data had attracted much attention in researchers. Radiative Transfer Equation (RTE) is used for linking LST to the TIR data [21]. Since the radiances calculated by the onboard satellite radiometers not only depend on the temperature and emissivity but also on atmospheric effects, it is difficult to obtain accurate data from TIR based LST estimation. Therefore, both emissivity, as well as atmospheric correction, need to be done for TIR based LST estimation. In LANDSAT-8 level-2 data, as already discussed, the images will be already atmospherically corrected. Based on the studies proposed by researchers for LST estimation, this can be mainly classified into two categories. The first one with known surface emissivity (SE) such as Single Channel (SC) algorithm, mono-window (MW) algorithm, split-window techniques [15, 22], multi-channel techniques [14]. The second category is with unknown SE as simultaneous retrieval of LST and emissivity with known atmospheric information, simultaneous retrieval with unknown atmospheric information, and stepwise retrieval method [23].

Users usually face some problems to estimate LST from the above techniques due to its complicated steps. Due to this, some researchers came up with some tools which use RS and GIS software such as ERDAS IMAGINE [2], ArcGIS [24], ENVI, Python, etc. for the estimation of LST [17]. ERDAS IMAGINE has got the MODEL MAKER tool, which helps in effective geospatial modeling, whereas ArcGIS helps in the proper analysis of the obtained data. In this paper, the ERDAS IMAGINE model maker tool and ArcGIS tool were used to develop geospatial modeling for automated LST estimation using the Single channel (SC) method and LANDSAT-8 data. In the SC method out of two thermal bands (band 10 and 11), only band-10 will be used for LST estimation. In addition to thermal bands, this method requires surface emissivity for the computation of LST. The surface emissivity was calculated using soil and vegetative indices. The obtained LST data were compared with 12 weather station point temperature data (obtained from KSNDMC). The detailed step by step procedure is explained further. The rest of the paper organized as follows: Section 2 describes the study area and data sets. The detailed methodology is in section 3. In section 4, results and discussion is given, and in section 5 conclusion is given.

2. Study Area and Datasets

Study area

The current study(as shown in Figure 1) was based on the Cauvery river basin [25] through Karnataka state, mainly the Mandya region. Cauvery river is one of the major rivers in India which originates at Talakaveri (12° 25′N, 75° 34′E) in Kodagu district, which is in the Western Ghats at an altitude 1341 m. The river basin is estimated to have an 8115 km^2 area, which occupies nearly 2.5% of the total geographical area of the country. Cauvery river basin catchment lies in Karnataka (41.2%), Tamil Nadu (55.5%), Kerala (3.3%).

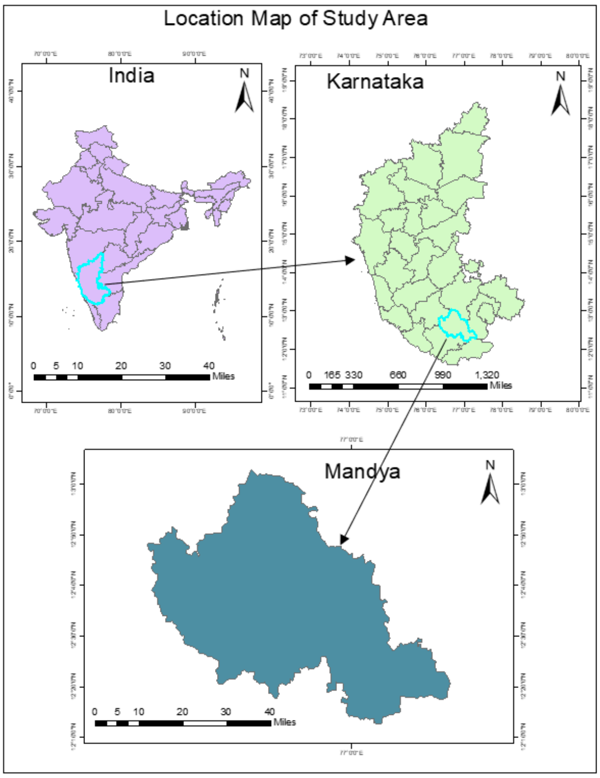

Fig. 1. Location map of the Study Area

Weather data

The weather data used in the present study was obtained from KSNDMC (Karnataka State Natural Disaster Monitoring Centre). The dataset consists of daily values of maximum and minimum temperature (T_{max}, T_{min}), which was used for comparing with the obtained surface temperature.

Satellite data

The LANDSAT-8 level 2 satellite images of the Mandya region (cloud-free data) were obtained from the USGS website as shown in Figure 2. LANDSAT-8 band designation is as in Table 1. Satellite images over the Mandya region of 21st January and 6th February 2018 have been used for this study (Table 2). The area of interest consists of a built-up area, vegetation, water, forest, grassland, bare soil, etc. *TIRS bands are acquired at 100m resolution, but in deliv-

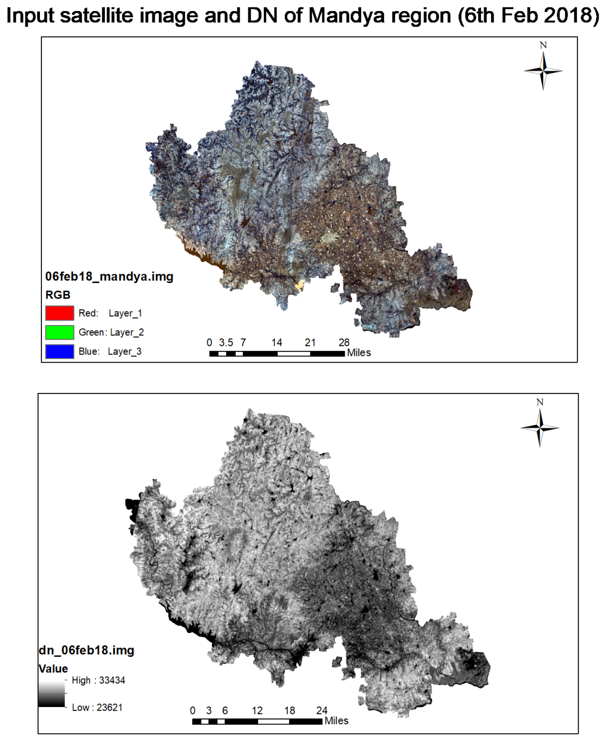

Fig. 2. Location map of the Study Area

Table 1. Technical specification of Landsat-8 [20]

Band	Spectral wavelength (m)	Resolution (m)
Band-1 (Coastal)	0.43-0.450	30
Band-2 (Blue)	0.45-0.51	30
Band-3 (Green)	0.533-0.59	30
Band-4 (Red)	0.63-0.67	30
Band-5 (Infrared)	0.85-0.87	30
Band-6 (Short wave) infrared SWIR 1)	1.56-1.65	30
Band-7 (Shortwave) Infrared SWIR2)	2.10-2.29	30
Band-8 (Panchromatic)	0.50-0.67	15
Band-9 (Cirrus)	1.36-1.38	30
Band-10 (TIRS1)	10.6-11.1	100 (30)*
Band-11 (TIRS2)	11.5-12.5	100 (30)*

ered data product, it is resampled to 30m.

3. Methodology

The methodology used for the study is as shown in the flowchart (Figure 3). LST estimation is done in the ERDAS Imagine model maker tool. LANDSAT-8 metadata used for this study is as shown in Table 4.

Step 1: Albedo (α)Calculation

Surface albedo is the ratio of radiation reflected from the surface to the shortwave radiation incident at the surface. For LANDSAT-8 shortwave spectrum (0.2 to 3.2µm) is represented by band 2-7. Albedo expression is given as in equation 1.

$$\alpha = \sum_{b=2}^{7} [\rho_{s,b} \cdot \omega_b] \tag{1}$$

here $\rho_{s,b}$ is the input satellite image reflectance of the area, as shown in Figure 2.

ω_b is the weighting coefficient of each band as given in Table 3.

Step 2: Vegetation Indices (NDVI, LAI) Calculation

Normalized Vegetation Indices (NDVI) indicates the vegetation cover of the region of interest and is calculated using band-4 and band-5 of Landsat-8 images using the equations 2 [7, 10, 18, 26]. In the electromagnetic spectrum, the near-infrared part reflects more energy by healthy vegetation. Its value ranges from -1 to +1. The value within 0.2 to +1 indicates green vegetation, and that which is less than 0, means water, snow, and clouds.

$$NDVI = \frac{(Band5 - Band4)}{(Band5 + Band4)} \tag{2}$$

NDVI obtained for the two dates are shown in Figure 4.

Leaf Area Index (LAI) is the ratio of the total area of all leaves on a plant to the ground area represented by the plant. It ranges from 0 to 6 and is expressed by using the empirical formula is given in equation 3 [27]. Along with NDVI, LAI for two dates is also shown in Figure 4.

$$LAI = 10NDVI_s^{3.5} \tag{3}$$

Step 3: Surface emissivity ($\epsilon_0, \epsilon_{\mathrm{NB}}$) Calculation

For LST estimation, it is necessary to obtain surface emissivity ($\epsilon_0, \epsilon_{\mathrm{NB}}$) [28]. Emissivity [29] helps in analyzing the amount of radiance emitted from the surface of the earth. It has more influence on LST. Based on the soil type, vegetation cover nature, and surface roughness, the surface emissivity is varied [3, 30, 31]. ϵ_0 is the broadband emissivity, and ϵ_{NB}, which is narrowband emissivity, is used for LST calculation. Surface emissivity is calculated using an empirical equation 4, 5 by [32] based on soil and vegetative indices.

For NDVI > 0

$$\epsilon_{NB} = 0.97 + 0.0033LAI \text{ for } LAI \leq 3 \tag{4}$$

$$\epsilon_{NB} = 0.98 \quad \text{ for } LAI > 3 \tag{5}$$

For NDVI ≤ 0

$$\text{Water } \alpha < 0.47_{NB} = 0.99 \tag{6}$$

$$\text{Snow } \alpha \geq 0.47_{NB} = 0.99 \tag{7}$$

The value of water and snow are set to the same in this study. But based on the locally calibrated emissivity value and user preference, this can be modified.

Step 4: Spectral radiance (L,) Calculation

As the satellite image used which is geometrically corrected data set; from that the DN(digital number) of band 10 is first converted to spectral radiance (L_λ) [29] using the equation 8

$$L_\lambda = M_L * Q_{cal} + A_L \tag{8}$$

Step 5: Land Surface Temperature (LST) Estimation

The last step is to obtain the land surface temperature (LST) [30, 33, 34] by using modified Plank is given in equation 9.

$$LST = \frac{K^2}{\ln\left(\frac{E_{NB}K_1}{L_\lambda} + 1\right)} \tag{9}$$

Where ϵ_{NB} is the narrow band emissivity, and Rc is the corrected thermal radiance from the respective surface. K1 and K2 values are constant, as in table 4. Finally, the satellite-derived land surface temperature is verified using weather station data, as shown in Table 5.

4. Results and Discussion

Two LANDSAT-8 images (as given in Table 2) of the Mandya region were taken from the USGS website for the study. The obtained image was layer stacked and applied mathematical models using the ERDAS IMAGINE tool. After getting the spectral radiance from the DN values, vegetation indices (NDVI, LAI), and surface albedo and emissivity were calculated. Weather station data was collected from KSNDMC and was used for comparing with the obtained surface temperature results for 12 representative points. Due to the variation in the resolution of LANDSAT-8, there can be a difference in the air temperature of a weather station and obtained surface temperature. It can be due to sensor characteristics as well as weather conditions.

The surface temperature of the Mandya region was calculated by processing LANDSAT-8 and by using equation 9 in the ERDAS IMAGINE model maker. Figures 5 & 6 display the surface temperature pattern of Mandya district for

Table 2. Satellite image details

DOY	Lat/Long	Acquisition dates	Path/Row	Local time
21	120 31′N, 76° 53′E	21/1/2018	144/51	10.40
37	120 31′N, 76° 53′E	06/2/2018	144/51	10.51

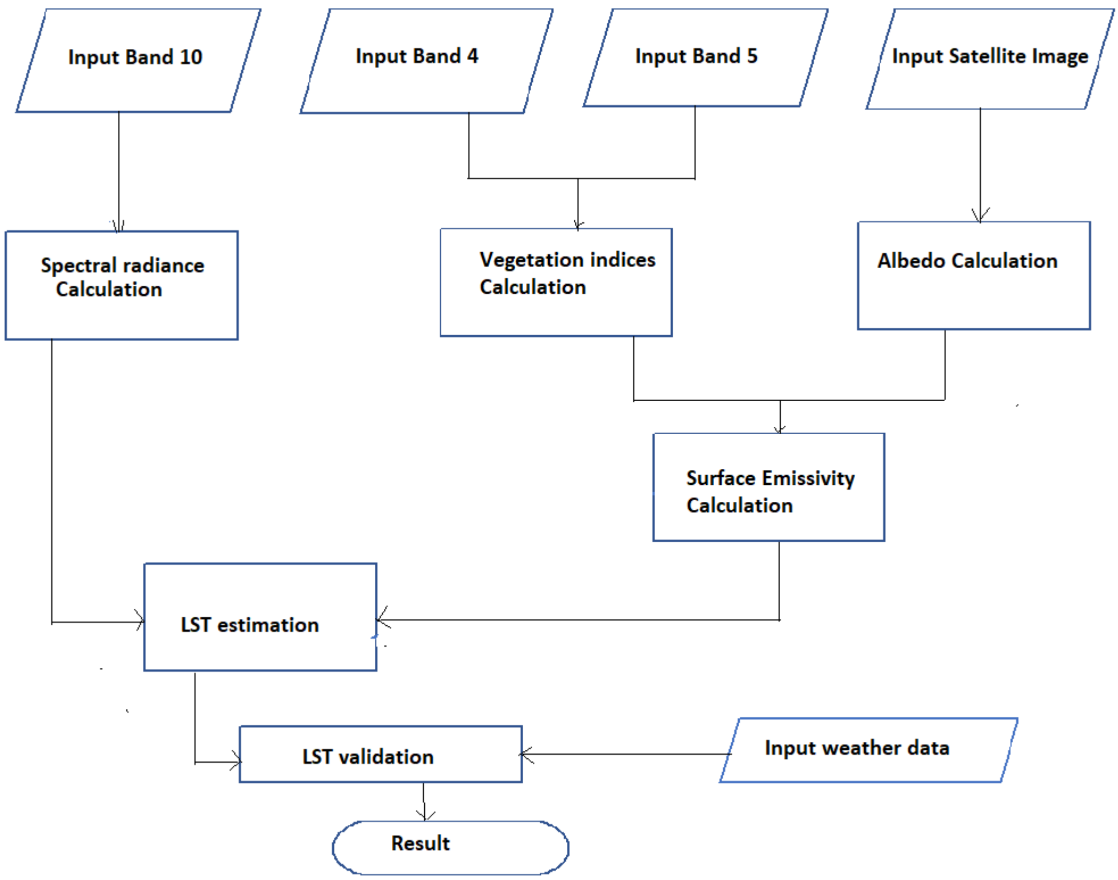

Fig. 3. Flow chart of LST estimation

Table 3. Weighing coefficient of LANDSAT-8 bands [20]

Term	Band-2	Band-3	Band-4	Band-5	Band-6	Band-7	Band-10
ω_b	0.254	0.149	0.147	0.311	0.103	0.036	0

21st Jan 2018 and 6th Feb 2018. In the figure, it is observed that the portion covered by vegetation is having a surface temperature value as low. In contrast, barren land and urban area are having the highest amount of surface temperature. As degree Celsius is used as a basic temperature unit for all analyses, the obtained LST value is converted to degree Celsius and shown here.

Comparison of estimated LST with the weather data:

For the region of interest, 12 points were selected for comparing LST and weather data. The difference between weather data and LST is shown in Table 5. It can be observed from the values that the obtained LST and weather data are following the same pattern for the selected 12 meteorological stations (Figure 7). The Root Mean Square Error (RMSE) and correlation coefficient (R) are used as statistical criteria for evaluating the model efficiency. From the comparison, it is found that RMSE and R for the first date are 0.94°C,0.62, and for the second date, it is 1.26°C,0.88, respectively. It is observed that LST and weather data are following the same pattern for the selected 12 meteorologi-

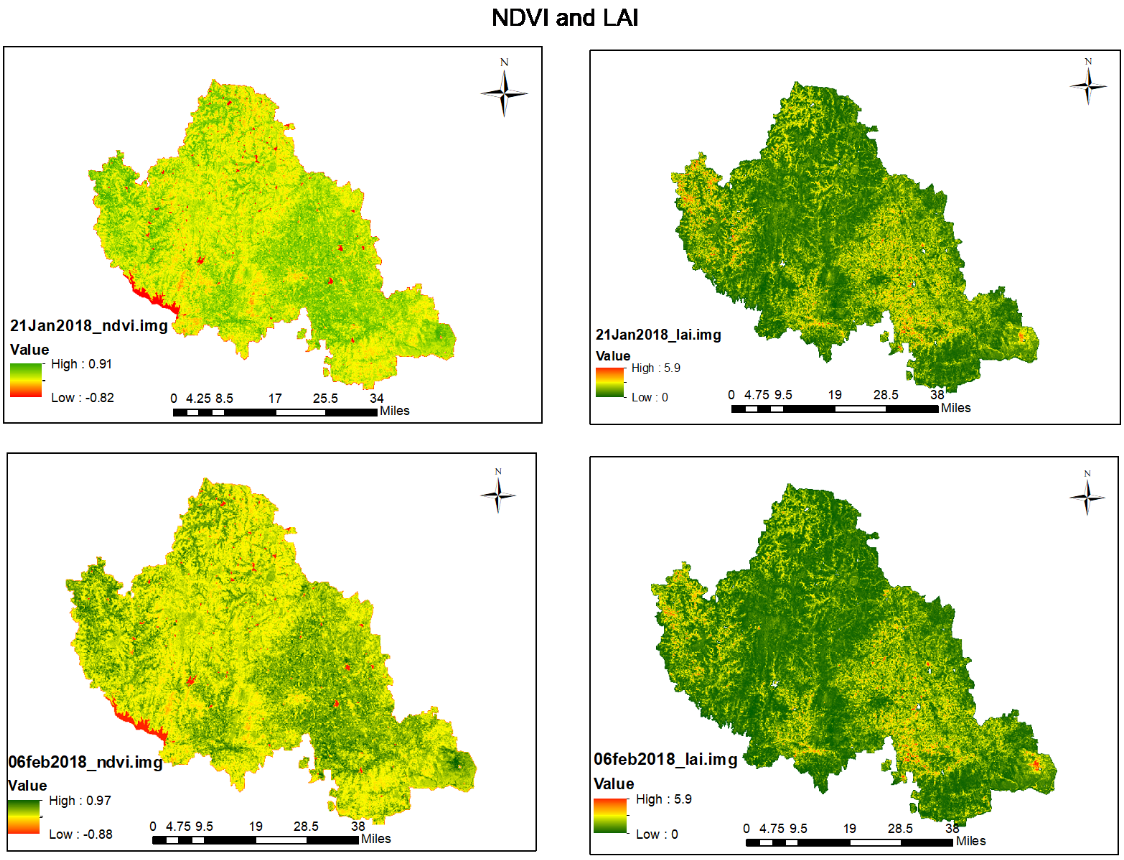

Fig. 4. Vegetation Indices values for 21st Jan 2018 6th Feb 2018

Table 4. LANDSAT-8 Metadata

Thermal Band	Variable	Description	Value
10	K1	Constant	774.8853
	K2		1321.0789
	M_L	RADIANCE$_M U$ LT$_B and$	0.00033420
	A_L	RADIANCE$_A D$ D$_B and$	0.1
	Q_{cal}	Pixel DN value	

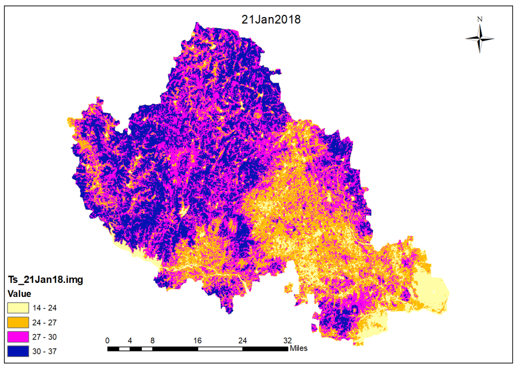

Fig. 5. Land Surface Temperature for 21st Feb 2018

cal stations.

$$RMSE = \sqrt{\frac{\sum (T_w - LST)^2}{n}} \qquad (10)$$

$$R = \frac{\sum (T_w - T_w')(LST - LST')}{\sqrt{\sum (T_w - T_w')^2}\sqrt{\sum (LST - LST')^2}} \qquad (11)$$

Where T_w and LST are the weather station temperature, and Land Surface Temperature, respectively, and n represents the number of points. T_w' and LST′ are mean weather station temperature and Land surface Temperature, respectively.

For the analysis of variation in the surface temperature of Mandya district, Karnataka, India, the remote sensing

Table 5. Weighing coefficient of LANDSAT-8 bands[20]

Sl No:	Location	Weather data (Temp °C)	LST (°C)	Difference	Weather data (Temp °C)	LST (°C)	Difference
		21st Jan 2018			6th Feb 2018		
1	Belluru	29.7	29	0.7	32.5	32	0.5
2	Bindiganavile	29.1	28	1.1	29.8	28	1.8
3	Kikkeri	30.8	31	-0.2	33.1	32	1.1
4	Krishnarajpet	30.5	31	-0.5	32.5	31	1.5
5	Akkehebbalu	30.4	30	0.4	33.5	32	1.5
6	Bukanakere	29.6	29	0.6	31.8	31	0.8
7	Sheelanere	30.7	29	1.7	32.4	31	1.4
8	Devalapura	30.6	29	1.6	33.5	33	0.5
9	Koppa	30	30	0	33.5	32	1.5
10	Athaguru	31.1	30	1.1	32.8	31	1.8
11	Maddur	30.2	30	0.2	32.3	31	1.3
12	Boppagowdanapura	30.2	29	1.2	31	31	0

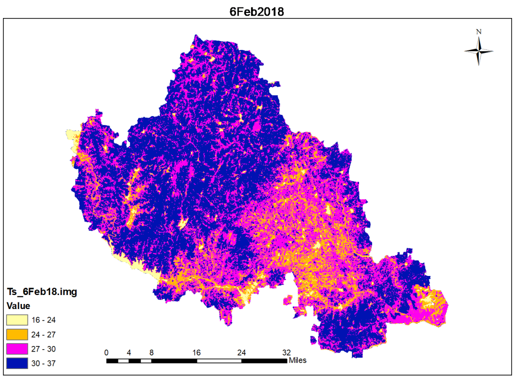

Fig. 6. Land Surface Temperature for 6th Feb 2018

techniques were used in the present study. The analysis of LST helps in understanding climate variations, which can also be used for understanding the urban heat island effect. It is seen that the vegetation and river basin areas that are acting as heat sink have a relatively lower temperature. The more vegetation leads to lower LST, as it enhances the ET that maintains the heat flux. It is also seen that for different LULC, LST and NDVI have different effects. The conclusion of this paper is summarized as follows:

5. Conclusion

The availability of remote sensing thermal data having high temporal and spatial resolution offers many opportunities. The TIR images correlated with weather station data allows the spatial distribution of LST to be modeled and estimated for the region of interest. It is observed that LST and weather data are following the same pattern for the selected 12 meteorological stations. The study results verified that LANDSAT-8 data could be further used for LST estimation of the Mandya region as well, extended to neighboring districts that lie on the Cauvery river basin. From the study, it is seen that as the vegetation index, i.e., as NDVI increases LST value has come down and vice versa. Thus, more green areas are recommended for controlling the land cover changes in the area of interest due to LST. We conclude that all the study results can be used for the development of both urban as well as the agricultural area of the Mandya district and its surroundings.

Acknowledgement

The authors are incredibly grateful to RRSC-South Bangalore for providing the resources to carry out the work. The LANDSAT-8 satellite data from USGS (US geological survey) and weather data from KSNDMC are acknowledged in this research.

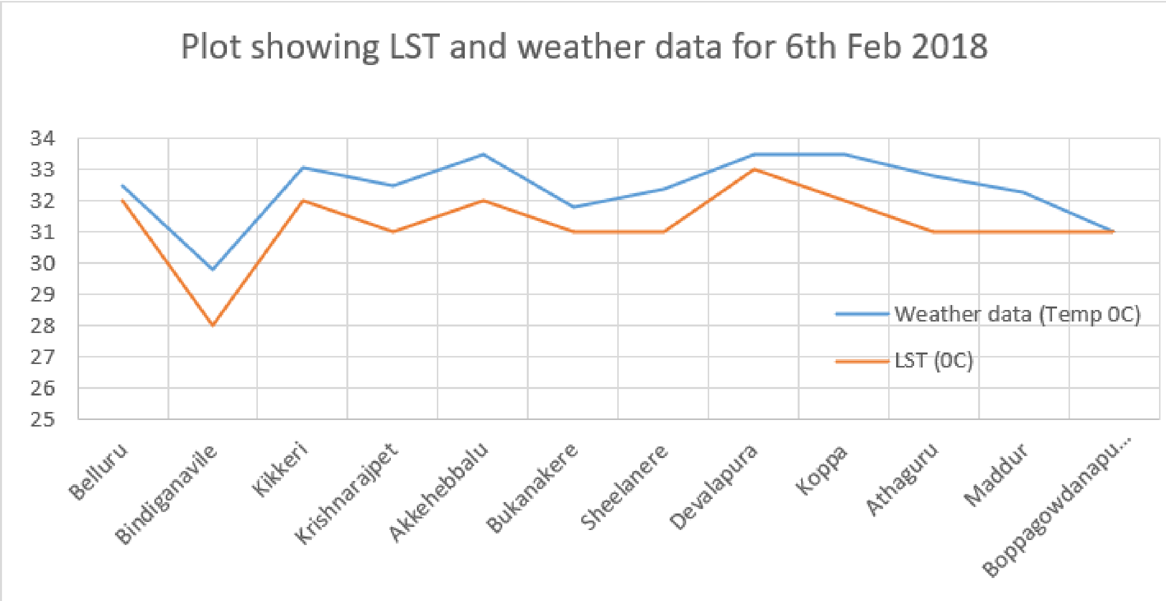

Fig. 7. Plot showing LST and weather data for 6^{th} Feb 2018

References

[1] M Bisquert, J. M. Sánchez, R. López-Urrea, and V. Caselles. Estimating high resolution evapotranspiration from disaggregated thermal images. *Remote Sensing of Environment*, 187:423–433, 2016.

[2] Qinqin Sun, Jianjun Tan, and Yonghang Xu. An ERDAS image processing method for retrieving LST and describing urban heat evolution: A case study in the Pearl River Delta Region in South China. *Environmental Earth Sciences*, 59(5):1047–1055, jan 2010.

[3] Marina Stathopoulou and Constantinos Cartalis. Daytime urban heat islands from Landsat ETM+ and Corine land cover data: An application to major cities in Greece. *Solar Energy*, 81(3):358–368, 2007.

[4] Stefania Bonafoni and Chaiyapon Keeratikasikorn. Land surface temperature and urban density: Multiyear modeling and relationship analysis using modis and landsat data. *Remote Sensing*, 10(9), 2018.

[5] Lidia Vlassova, Fernando Pérez-Cabello, Marcos Rodrigues Mimbrero, Raquel Montorio Llovería, and Alberto García-Martín. Analysis of the relationship between land surface temperature and wildfire severity in a series of landsat images. *Remote Sensing*, 6(7):6136–6162, 2014.

[6] Salman Özupekce. Use of Land Surface Temperature (Lst) Data in the Determination of High Areas of Forest Fire Risk in Erdemli District. *Journal of International Social Research*, 11(57):227–232, 2018.

[7] Ruyan He, Yufang Jin, Maziar M Kandelous, Daniele Zaccaria, Blake L Sanden, Richard L Snyder, Jinbao Jiang, and Jan W Hopmans. Evapotranspiration estimate over an almond orchard using Landsat satellite observations. *Remote Sensing*, 9(5), 2017.

[8] B. N. Aryalekshmi, Rajashekhar C. Biradar, and J. Mohammed Ahamed. Thermal imaging techniques in agricultural applications. *International Journal of Innovative Technology and Exploring Engineering*, 8(12):2162–2168, oct 2019.

[9] Ann Kathrin Holtgrave, Michael Förster, Felix Greifeneder, Claudia Notarnicola, and Birgit Kleinschmit. Estimation of Soil Moisture in Vegetation-Covered Floodplains with Sentinel-1 SAR Data Using Support Vector Regression. *PFG - Journal of Photogrammetry, Remote Sensing and Geoinformation Science*, 86(2):85–101, apr 2018.

[10] Syed Muhammad Zubair Younis and Javed Iqbal. Estimation of soil moisture using multispectral and FTIR techniques. *Egyptian Journal of Remote Sensing and Space Science*, 18(2):151–161, 2015.

[11] S K Dash and J. C.R. Hunt. Variability of climate change in India, 2007.

[12] Lingli Wang and John J. Qu. Satellite remote sensing applications for surface soil moisture monitoring: A review, 2009.

[13] Ricardo Trezza, Richard G Allen, and Masahiro Tasumi. Estimation of actual evapotranspiration along the Middle Rio Grande of New Mexico using MODIS and landsat imagery with the METRIC model. *Remote*

Sensing, 5(10):5397–5423, 2013.

[14] Geng Ming Jiang and Ronggao Liu. Retrieval of sea and land surface temperature from SVISSR/FY-2C/D/E measurements. *IEEE Transactions on Geoscience and Remote Sensing*, 52(10):6132–6140, 2014.

[15] C. Ottlé and D Vidal-Madjar. Estimation of land surface temperature with NOAA9 data. *Remote Sensing of Environment*, 40(1):27–41, 1992.

[16] A Rajeshwari. ESTIMATION OF LAND SURFACE TEMPERATURE OF DINDIGUL DISTRICT USING LANDSAT 8 DATA. *International Journal of Research in Engineering and Technology*, 03(05):122–126, 2014.

[17] Ugur Avdan and Gordana Jovanovska. Algorithm for automated mapping of land surface temperature using LANDSAT 8 satellite data. *Journal of Sensors*, 2016, 2016.

[18] Emily G. Kullberg, Kendall C. DeJonge, and José L. Chávez. Evaluation of thermal remote sensing indices to estimate crop evapotranspiration coefficients. *Agricultural Water Management*, 179:64–73, 2017.

[19] William Kustas and Martha Anderson. Advances in thermal infrared remote sensing for land surface modeling. *Agricultural and Forest Meteorology*, 149(12):2071–2081, 2009.

[20] USGS. Landsat Missions, 2019.

[21] Larry M. McMillin. Estimation of sea surface temperatures from two infrared window measurements with different absorption. *Journal of Geophysical Research*, 80(36):5113–5117, dec 1975.

[22] Offer Rozenstein, Zhihao Qin, Yevgeny Derimian, and Arnon Karnieli. Derivation of land surface temperature for landsat-8 TIRS using a split window algorithm. *Sensors (Switzerland)*, 14(4):5768–5780, 2014.

[23] Zhao Liang Li, Bo Hui Tang, Hua Wu, Huazhong Ren, Guangjian Yan, Zhengming Wan, Isabel F. Trigo, and José A. Sobrino. Satellite-derived land surface temperature: Current status and perspectives, 2013.

[24] ARCGIS. Chapter 5 Geospatial Modeling 5.1 Rationale 5.2 SEBAL modeling for evapotranspiration 5.3 Penman-Monteith method for evapotranspiration 5.4 Runoff modeling 5.5 Recharge modeling 5.6 Weighed Overlay Analysis using GIS 5.1 Rationale. Technical report.

[25] H. R. Shwetha and D. Nagesh Kumar. Performance evaluation of satellite-based approaches for the estimation of daily air temperature and reference evapotranspiration. *Hydrological Sciences Journal*, 63(9):1347–1367, jul 2018.

[26] Athos Agapiou, Nikos Papadopoulos, and Apostolos Sarris. Monitoring olive mills waste disposal areas in Crete using very high resolution satellite data. *Egyptian Journal of Remote Sensing and Space Science*, 19(2):285–295, 2016.

[27] W G M Bastiaanssen. *Remote Sensing in Water Resources Management : The State of the Art*. 1998.

[28] José A. Sobrino, Juan C. Jiménez-Muñoz, Guillem Sòria, Mireia Romaguera, Luis Guanter, José Moreno, Antonio Plaza, and Pablo Martínez. Land surface emissivity retrieval from different VNIR and TIR sensors. In *IEEE Transactions on Geoscience and Remote Sensing*, volume 46, pages 316–327, 2008.

[29] Kalifa Goïta and Alain Royer. Surface temperature and emissivity separability over land surface from combined tir and swir avhrr data. *IEEE Transactions on Geoscience and Remote Sensing*, 35(3):718–733, 1997.

[30] Andrew M. Coutts, Richard J. Harris, Thu Phan, Stephen J. Livesley, Nicholas S.G. Williams, and Nigel J. Tapper. Thermal infrared remote sensing of urban heat: Hotspots, vegetation, and an assessment of techniques for use in urban planning. *Remote Sensing of Environment*, 186:637–651, 2016.

[31] De Cai Wang, Gan Lin Zhang, Ming Song Zhao, Xian Zhang Pan, Yu Guo Zhao, De Cheng Li, and Bob Macmillan. Retrieval and mapping of soil texture based on land surface diurnal temperature range data from MODIS. *PLoS ONE*, 10(6), 2015.

[32] Masahiro Tasumi, Richard G Allen, Ricardo Trezza, and James L Wright. Satellite-based energy balance to assess within-population variance of crop coefficient curves. *Journal of Irrigation and Drainage Engineering*, 131(1):94–109, jan 2005.

[33] Rizqi I. Sholihah, Bambang H. Trisasongko, Diar Shiddiq, La Ode S. Iman, Selamet Kusdaryanto, Manijo, and Dyah R. Panuju. Identification of Agricultural Drought Extent Based on Vegetation Health Indices of Landsat Data: Case of Subang and Karawang, Indonesia. *Procedia Environmental Sciences*, 33:14–20, 2016.

[34] Anju Bala, Prakashkiran S Pawar, Anil Kumar Misra, and Kishan Singh Rawat. Estimation and validation of actual evapotranspiration for wheat crop using SEBAL model over Hisar district, Haryana, India. *Current Science*, 113(1):134–141, 2017.